SAND2007-4874C

July 27, 2007 (revised) – ICDS-24 – X05-3

# Modeling fast-transient defect evolution and carrier recombination in pulse-neutron-irradiated Si devices

S. M. Myers, W. R. Wampler, P. J. Cooper, and D. B. King

Sandia National Laboratories, Albuquerque, New Mexico

This work explores the feasibility of mechanistically modeling the transient behavior of defects and carriers in bipolar Si devices exposed to pulses of MeV neutrons. Our approach entails a detailed, finite-element treatment of the diffusion, field-drift, and reactions of well established primal defects and reacted states, taking into account the localization of displacement damage within secondary cascades. The modeling captures a variety of the properties of pulse-neutron-irradiated transistors observed from electrical measurements and deep-level transient spectroscopy, using parameter values consistent with independently available information.

Keywords: silicon; defects; modeling; transistor

Corresponding author: Samuel M. Myers

Org. 01112 / Mail Stop 1056

Sandia National Laboratories

P.O. Box 5800

Albuquerque, New Mexico 87185 - 1056

FAX 505-844-7775

EMAIL smmyers@sandia.gov

## 1. Introduction

Describing the time-dependent properties of a neutron-irradiated Si device in terms of underlying atomic processes is challenging in several respects. Understanding of the isolated primal defects – as produced, for example, by electron bombardment – is extensive but nevertheless incomplete. Moreover, the values of such key parameters as diffusion coefficients and cross sections for carrier capture are not well known in many cases. Added to this is the localization of MeV-neutron damage in recoil cascades, altering reaction rates and charge states and producing local fields that influence the interactions with carriers. Further, there is the possibility of still-to-be-characterized electrically active species within the central regions of clusters or associated with amorphized regions. Such considerations suggest that quantitative prediction based solely upon atomistic information from independent sources is unrealistic. Heretofore, transient irradiation behavior has been described by phenomenological models fitted to irradiation testing as close as possible to conditions of interest. [Refs. 1,2 and citations therein.]

We are exploring whether models based upon well established defects and atomic processes can capture the dominant influences on irradiated-device behavior, replicate major observed trends, and approach quantitative consistency with experiment through adjustment of inaccurately known parameters within realistic bounds. Such modeling should test present understanding and illuminate the interplay between microscopic processes and macroscopic device behavior, and it may facilitate more robust extrapolation from irradiation testing. In this article we outline the methodology and present initial findings, with a full description to be published later.

## 2. Method

Our modeling begins with the determination of spherically symmetric concentration profiles for the primal vacancies and interstitials within an idealized recoil cascade that is statistically representative of the neutron-irradiated Si. This is accomplished through pair-correlation-function analysis of defect maps generated by the binary-collision code MARLOWE [3], as applied to a spectrum of primary Si-recoil energies appropriate for a well characterized pulse reactor (SPR-III at Sandia) [4]. The radial

concentration profile of vacancies is chosen so that the vacancy-vacancy correlation function obtained from that profile is the same as the corresponding correlation function from the defect map, with a similar procedure being used to determine the interstitial concentration profile. The resultant radial distributions are positioned within a microscopic spherical volume with boundary at radius R = 0.5 μm; this volume also contains uniformly distributed B and P dopants and O and C impurities. Interaction with the surrounding device environment is via the control of carrier concentrations at the boundary. The ensuing time-evolution of this microscopic volume, along with the device-degrading in-flow of carries due to recombination at the defects, is modeled by solving a system of coupled differential equations – one for each carrier and each charge state of the multiple defect species – that gives the changes in concentration arising from diffusion, field-drift, and reactions. Poisson's equation is solved at each time step.

Modeling of the time-evolution of the above cluster included defect species judged from the literature to be relevant at a temperature of 300 K and times < 1 s. [Refs. 5,6 and citations therein.] These include the monovacancy (V) with charge states from +2 to –2; the divacancy (VV) for +1 to –2; the complexes VP (+1 to –1) and VO (0, –1); the Si interstitial ($Si_I$) for +2 to –2; the B interstitial ($B_I$) for +1 to –1 and its complexes with O (0, –1) or with a second B (+1, 0); and interstitial C ($C_I$) for +1 to –1. Diffusion was implemented for V, $Si_I$, and $B_I$. Including the two carriers and the unreacted dopants and impurities, the concentrations of 37 species were followed in the calculation. Most bandgap levels and the diffusion coefficients of V and B were obtained from the literature [Refs. 5,6 and citations therein]; the properties of $Si_I$ , where experiments are not available, were calculated by N. A. Modine using density-functional theory [7]. Defect reactions (with species other than carriers) involving electrostatic attraction were assigned effective radii corresponding to the distance at which the binding energy equals kT, whereas defect reactions with electrostatic repulsion were neglected. In the absence of electrostatic interaction, the effective radius was one lattice parameter, except in the case of the strongly strain-affected annihilation of interstitial-type defects with vacancy defects, where a value of

2 nm was used. Cross-sections for carrier capture by defects were equated to representative, rule-of-thumb values: $3\times10^{-16}$ cm$^2$ when the trap and carrier have the same charge sign; $3\times10^{-15}$ cm$^2$ when the trap is neutral; and $3\times10^{-14}$ cm$^2$ for opposite signs. The vacancy defects present at zero time were apportioned between V and VV according to the ratio [VV] / [V] = 0.23, while all of the interstitials were taken to be isolated, in accord with results obtained by S. M. Foiles using molecular dynamics [8].

**3. Results and discussion**

We now present modeling results for three microscopic regions of a specific bipolar junction transistor (Microsemi 2N2222), and comment upon the predicted behavior and its consistency with experimental information. This vertically layered n-p-n device has a highly doped emitter and lower doped base formed by overlapping diffusion profiles of P and B, and these are located in the upper region of a lightly p-doped epi layer atop $n^+$ material.

Figure 1 shows radial concentration profiles of the dominant constituents within the modeled spherical volume for the case where it resides at the emitter-base junction, both at times immediately following the formation of the recoil cascade and after the system has evolved for 1 s at 300 K. The local concentrations of B and P at the junction are $1\times10^{17}$ cm$^{-3}$, while the impurity levels are $2\times10^{17}$ O cm$^{-3}$ and $1\times10^{16}$ C cm$^{-3}$. The junction is considered to be forward-biased at 0.6 V, implying local electron and hole concentrations of about $7\times10^{14}$ cm$^{-3}$, which is taken as the boundary condition at R = 500 nm for the modeled volume. The diffusion and reactions of $Si_I$ and then V lead to relatively rapid defect recombination in the high-concentration core of the cluster, followed more slowly by outward migration of the surviving species to form, predominantly, VP and $B_I$; the subsequent migration and reactions of $B_I$ at 300 K are inconsequential for times < 1 s. Of the approximately 568 Frenkel pairs initially present within the cluster, about 30% have escaped recombination at 1 s, producing 84 VP, 37 VV, and 151 $Bi_I$ along with smaller components of VO (10)and $C_I$ (15). The predicted apportioning of vacancies among reacted states is roughly consistent with experimental studies of the junction in question using deep-level transient spectroscopy (DLTS) by R. M. Fleming *et al*. [9], who inferred the

dominance of VP with a possible secondary contribution from VV. Vacancy-interstitial recombination is strongly enhanced by the localization of the primal defects within the recoil cascade; a similar calculation with the same number of defects dispersed randomly showed recombination removing only about 3% of the defects.

Figure 2 shows the predicted variation with time of the principal defects within the modeled spherical cluster when it resides in the neutral, p-type base of the transistor, with the emitter-base junction again being under a forward bias of 0.6 V. The local dopant concentrations are now $2.1\times10^{16}$ B $cm^{-3}$ and $1\times 10^{15}$ P $cm^{-3}$; the hole concentration is $2\times10^{16}$ $cm^{-3}$ and the electron concentration $6\times10^{12}$ $cm^{-3}$. For this region and operating condition, several complicating factors are simultaneously prominent, making the modeling particularly complex and informative. For example, the interstitial and vacancy diffuse at comparable rates, making them active within the same time interval. Moreover, these diffusion rates fall off rapidly with distance from the center of the cluster, mainly due to a shift toward less mobile charge states, so that the evolution is extended in time. And, the enhancement of carrier recombination by band-bending in the cluster is much more pronounced in the neutral zone than at the carrier-depleted emitter-base junction.

The consequences for device operation are reflected in Fig. 3, which shows the total flow of carriers into the cluster versus time. Also given is the result when the same number of defects is uniformly dispersed within the modeled sphere. In the latter case, the much smaller variation in defect mobilities and the absence of band-banding result in a sharp recovery stage. The two curves in Fig. 4 closely resemble a reported comparison between the time-dependent carrier lifetimes measured in p-type Si after pulse irradiation with neutrons or electrons [10].

The time-dependent behavior of the spherical cascade was also modeled for conditions representing the lightly doped ($5\times10^{14}$ $cm^{-3}$) region of the n-type collector, now with equilibrium carrier concentrations at the boundary corresponding to zero-bias conditions. After 1 s at 300 K, the dominant reaction products from the 568 initial Frenkel pairs are VV (23), VO (72), and $C_I$ (118), with the number

of VP being only about 3. The great reduction in VP from the emitter-base junction, and the comparable numbers of VV and VO, are in approximate accord with DLTS measurements on the same device by R. M. Fleming *et al*. [9].

Under the conditions of DLTS experiments, the time dependent rate of conversion from $VV^{-1}$ to $VV^{-2}$ during the zero-bias filling pulse is sensitive to the VV clustering. This is due to local band-bending, which reduces the carrier concentration at the clustered defects by an amount dependent upon location, typically giving rise to a roughly logarithmic time dependence. Figure 4 shows modeling results for the $VV^{-1}$ to $VV^{-2}$ conversion at 135 K, following the aforementioned evolution for 1 s at 300 K. Also given is the modeled behavior without clustering, where the charging occurs more rapidly and in a sharper stage. The character of the time dependence is in accord with experimental data for the same device obtained by Fleming *et al*. [11], which are included in Fig. 5; the offset in time may relate to the capture cross-section used as well as other aspects of the modeling.

The above treatment of microscopic clusters at various locations in the transistor could be incorporated into a finite-element model of the macroscopic device via position- and time-dependent carrier lifetimes derived from the predicted flows into the clusters such as that in Fig. 3. We have instead begun with a simplified treatment in which 1) the irradiation damage is restricted to the vicinity of the emitter-base junction, where the sensitivity to displacement damage is greatest and the effects of band bending in the cluster are relatively small; 2) the defects are randomly distributed rather than clustered, and the rapid initial recombination of vacancies and interstitials within the clusters is accounted for by a reduction of their starting concentrations; and 3) carrier flows within the device are treated in a one-dimensional approximation. The equations describing the diffusion, drift, and reactions of carriers and defects are then applied directly to the operating macroscopic device.

Comparisons with experiment for the n-p-n transistor appear in Fig. 5, which shows the ratio of base current to collector current (reciprocal gain) versus time for fixed emitter current. The ~100-μs neutron-irradiation pulse is manifested by the negative excursion due to gamma-induced photocurrent.

In order to improve the agreement, carrier-capture cross-sections for the V and VP were modified by as much as a factor of 6 from nominal values, and the diffusion coefficient of $V^{-2}$ was reduced by a factor of 10 from an extrapolation of cryogenic experiments; both of these adjustments are considered compatible with available information. The same parameter values were used throughout. The extension of the recovery over several decades in time emerges naturally from the widely varying population of the relatively mobile $V^{-2}$ state across the emitter-base junction, where the concentrations of electrons and holes change rapidly with depth. The model calculations capture major features of the observed behavior.

## 4. Conclusions

In this paper we have outlined an approach for atomistic modeling of defect and carrier behavior in Si devices under pulsed neutron irradiation. The method treats the collisional processes giving rise to primal defects, proceeds to a finite-element description of the subsequent transport and reactions of the defects and carriers, and extends ultimately to device operation. We believe that modeling results and comparisons with experiment to date support the view that major trends, and possibly even quantitative behavior, may ultimately be captured by such calculations using physically reasonable adjustment of parameters.

## Acknowledgements

This work was supported by the Sandia National Laboratories program on Qualification Alternatives to the Sandia Pulse Reactor (QASPR). Sandia is a multiprogram laboratory operated by Sandia Corp., a Lockheed Martin Company, for the U.S. D.O.E. under Contract DE-AC04-94AL85000.

## References

[1] G. C. Messenger and M. S. Ash, The Effects of Radiation on Electronic Systems (Van Nostrand Reinhold, New York, 1992) pp. 192-268.

[2] J. R. Srour, C. J. Marshall, and P. W. Marshall, IEEE Trans. Nucl. Sci. 50 (2003) 653.

[3] M. T. Robinson, Nucl. Instrum. Meth. B 67 (1992) 396.

[4] J. G. Kelly, P. J. Griffin, and W. C. Fan, IEEE Trans. Nucl. Sci. 40 No. 6 (1993) 1418.

[5] G. D. Watkins, in: Crystalline Silicon, ed. R. Hull (INSPEC, London, 1999) pp. 643-652.

[6] P. Pichler, Intrinsic Point Defects, Impurities, and Their Diffusion in Silicon (Springer, New York, 2004).

[7] N. A. Modine, present proceedings.

[8] S. M. Foiles, Nucl. Instrum. Meth. B 255 (2007) 101, and private communication.

[9] R. M. Fleming, private communication.

[10] Reference 2, Fig. 2.

[11] R. M. Fleming, C. H. Seager, D. V. Lang, P. J. Cooper, E. Bielejec, and J. M. Campbell, J. Appl. Phys., in press.

**Figure captions**

Fig. 1. Radial concentration profiles of selected defects within the spherical cluster at zero time and after thermal evolution at 300 K for 1 s, for the emitter-base junction.

Fig. 2. Defect numbers within the spherical cluster at 300 K for the neutral base.

Fig. 3. Flow of electrons into the cluster due to recombination at defects for the experiment of Fig. 3, compared to the case for uniformly dispersed defects.

Fig. 4. Fraction of divacancies in the –2 charge state versus time during a DLTS filling pulse at 135 K. The DLTS signal is scaled to the modeled charged fraction at long times.

Fig. 5. Ratio of base current to collector current versus time for the n-p-n transistor operating at two emitter currents.

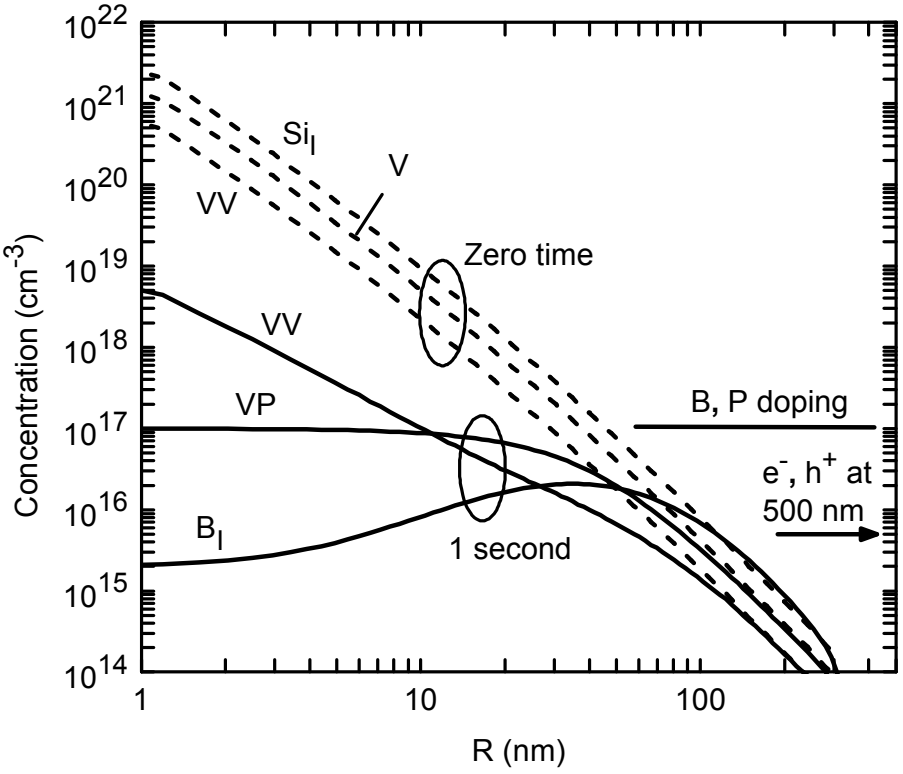


Figure 1

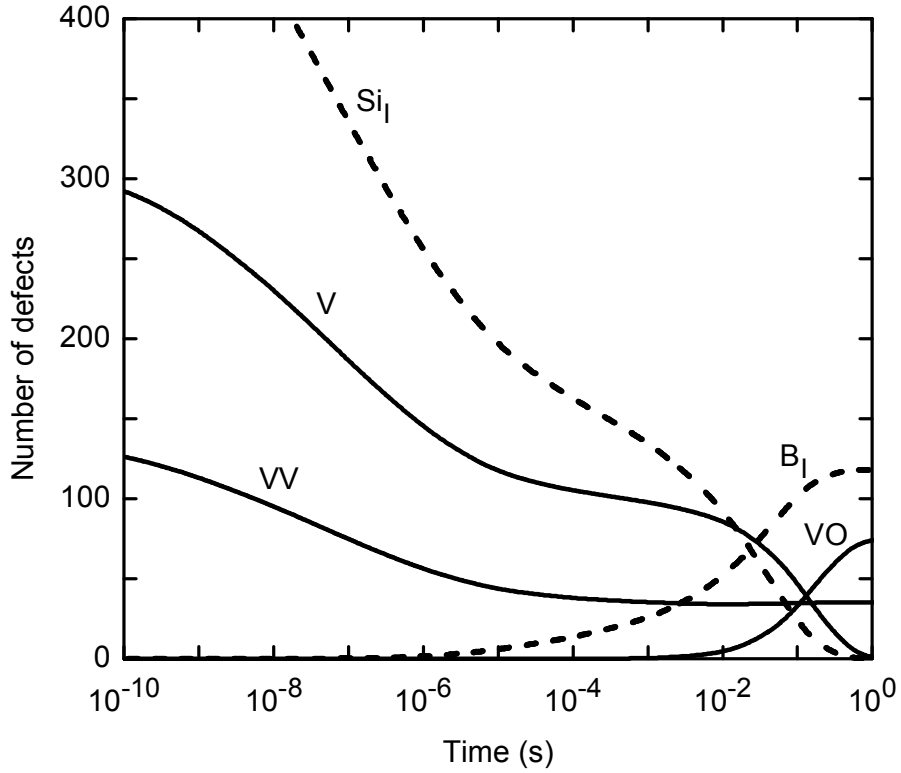


Figure 2

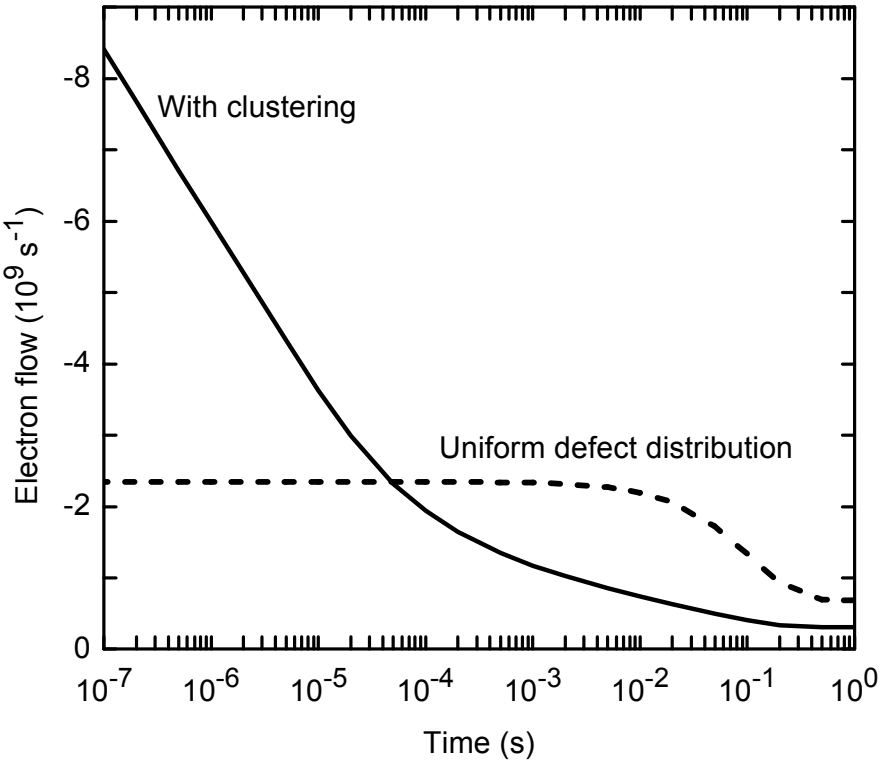


Figure 3

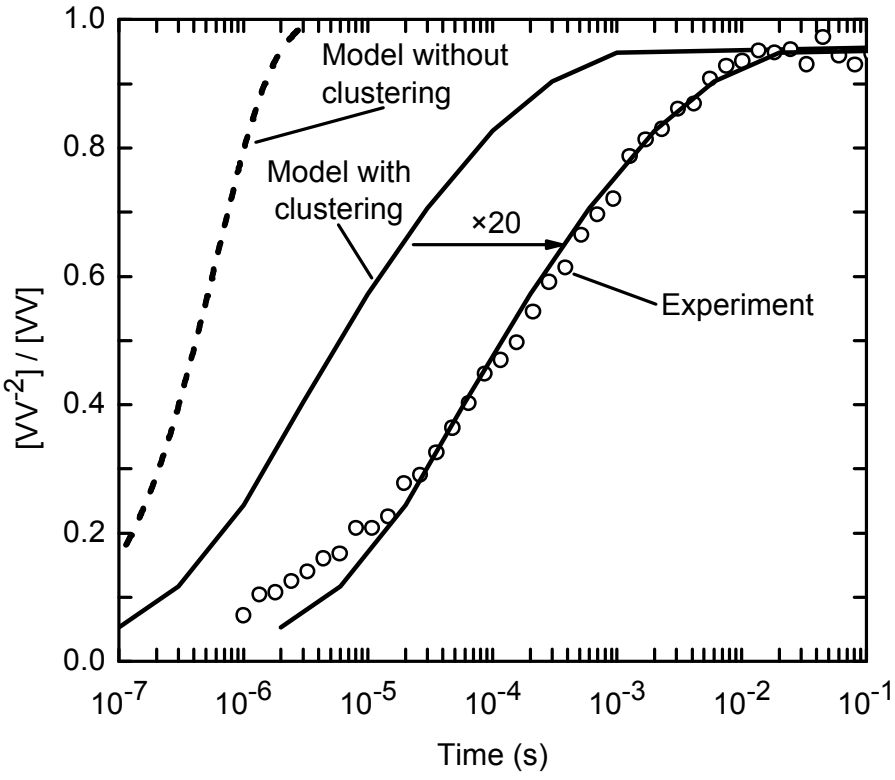


Figure 4

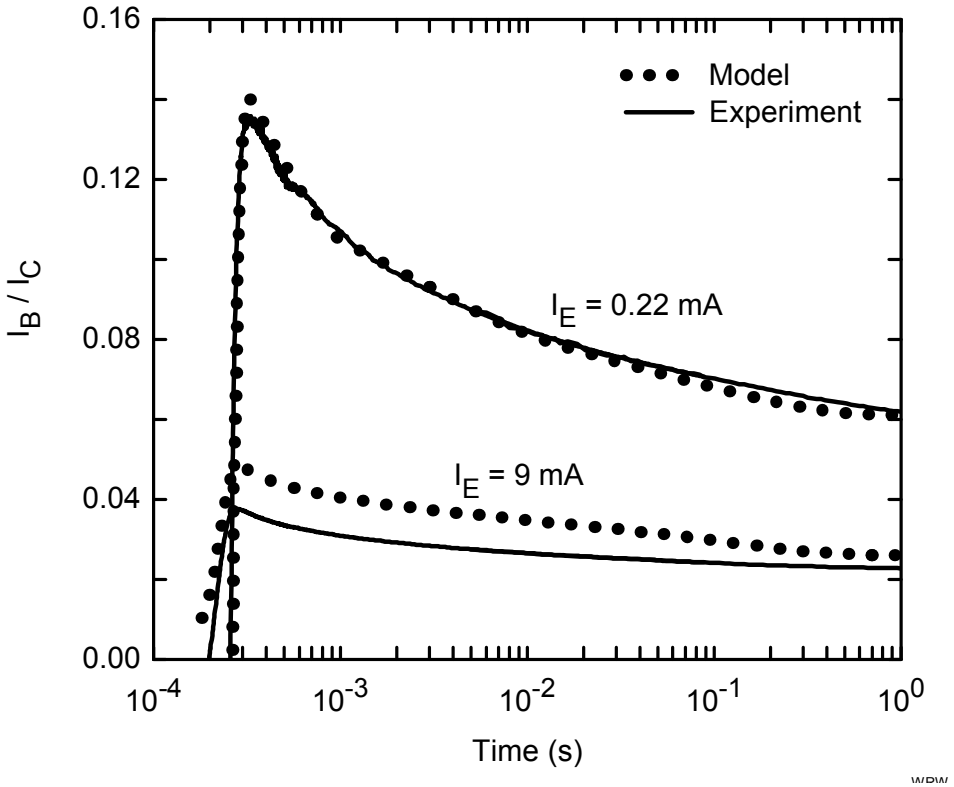
0.16
0.12
0.08
0.04
0.00
$I_B / I_C$
Model
Experiment
$I_E$ = 0.22 mA
$I_E$ = 9 mA
$10^{-4}$
$10^{-3}$
$10^{-2}$
$10^{-1}$
$10^{0}$
Time (s)

Figure 5